Supplementary Material

Utilization of a Regional Dew Formation Model in Kenya

Atashi et al.

Table S1: Dew yield from plane radiative condensers in various field campaigns and models.

Sampling site	Dew events	Study period	Mean volume [L/m2/day]	Max volume [L/m2/ day]	Observed/ Modeled	Reference
Fayetteville, AR (USA)	107	Jul 1989–July 1990	0.15	-	Obs	Wagner et al. (1992)
Dodoma (Tanzania)	-	30 nights	0.04	-	Obs	Nilsson (1994)
Kungsbacka (Sweden)	11	14 Aug–01 Sept 1993	0.145	0.21	Obs	Nilsson, (1996)
Dodoma (Tanzania)	21	Nov 1993	0.057	0.08	Obs	Nilsson, (1996)
Dodoma (Tanzania)	147	25 Aug 1994–4 Feb 1995	0.05	0.24	Obs/Mod	Vargas et al. (1998)
Sde Boqer (Israel)	34	Aug–Nov 1992	0.2/dew&fog	-	Obs	Kidron (1999)
Har Harif (Israel)	21	Aug–Nov 1992	0.3/dew&fog	-	Obs	Kidron (1999)
Dayalbagh (India)	-	15 Dec–15 Feb	0.59	1.38	Obs	Khare et al. (2000)
Ajaccio (France)	214	22 July 2000–11 Sept 2001	0.12	0.38	Obs	Muselli et al. (2002)
Osaka (Japan)	16	No info	0.14	-	Obs	Takenaka et al. (2003)
Grenonle (France)	109	25 Nov1999– 23 Jan 2001	0.036	-	Obs	Beysens et al. (2003)
Zadar (Croatia)	87	21 July 2003–31 May 2004	0.15	-	Obs	Mileta et al. (2004)
Jerusalem (Israel)	176	01 June 2003–31 May 2004	0.188	~ 0.50	Obs	Berkowicz et al. (2004)
Komiz˘a (Croatia)	76	24 June 2003–26 April 2004	0.08	-	Obs	Mileta et al. (2004)
Bordeaux (France)	211	14 Aug 1999–23 Jan 2001	0.046	-	Obs/Mod	Beysens et al. (2005)
Dhahran (Saudii Arabia)	-		0.22	-	Obs/Mod	Gandhisan and Abualhamayel (2005)
Brive-la-Gaillarde (France)	275	01 Jan–31 Dec 2000	0.115	<0.475	Obs	Beysens et al. (2006a)
Ajaccio (France)	-	10 Dec 2001–10 Dec 2003	~ 0.106	~ 0.332	Obs	Muselli et al. (2006a)
Bordeaux (France)	110	15 Jan 2002–14 Jan 2003	-	~ 0.22	Obs	Beysens et al. (2006b)
Jerusalem (Israel)	554	2003–2006	0.199	~ 0.60	Obs	Berkowicz et al. (2007)
Kothara (India)	-	01 Oct 2004–31 May 2005	0.098	0.24	Obs	Sharan et al. (2007)
Central Netherlands	-	Dec 2003–May 2005	0.10	-	Obs	Jacobs et al. (2008)
Tahiti	151	16 May–14 Oct 2005	0.068	0.22	Obs	Clus et al. (2008)
Tikehau	109	21 June–07 Oct 2005	0.102	0.23	Obs	Clus et al. (2008)
Komiz˘a (Croatia)	263	07 Jan 2003–31 Oct 2006	0.108	0.592	Obs	Muselli et al. (2009)
Zadar (Croatia)	484	07 Jan 2003–31 Oct 2006	0.138	0.406	Obs	Muselli et al. (2009)
South–West Morocco	178	01 May 2007–30 April 2008	0.106	-	Obs	Lekouch et al. (2010a)
Wrocław (Poland)	421	05 Oct 2007–07March 2010	0.103	0.354	Obs	Sobik et al. (2010)
Sudetes (Poland)	55	21 June 2009–16 Jan 2010	0.190	0.452	Obs	Sobik et al. (2010)
Cartagena (Spain)	175	May 2009–May 2010	0.105	-	Obs	Maestre-Valero et al. (2011)
Panandhro (India)	69	07 Feb 2004–25Feb 2006	0.189	-	Obs	Sharan et al. (2011)
Mirleft (Morocco)	178	01 May 2007–30 April 2008	0.106	-	Obs/Mod	Lekouch et al. (2012)
Id Ouasskssou (Morocco)	187	01 May 2007–30 April 2008	0.202	-	Obs	Lekouch et al. (2012)
Wroclaw (Poland)	19	April–Sep 2009	0.179	-	Obs	Galek et al. (2012)
Sde Boqer (Israel)	29	during the fall of 1992	0.21	-	Obs	Kidron & Starinsky (2012)
Idouasskssou (Morocco)	137	15 Dec 2008–31 July 2009	0.158	-	Obs	Clus et al. (2013)
Adelaide Hills (Australia)	14	24 April–23 May 2009	0.225	-	Obs/Mod	Guan et al. (2014)
Mexico City (Mexico)	-	22 Dec 201–21 Mar 2012	0.0317	-	Obs	Arias-Torres & Flores-Prieto (2015)
Krakow (Poland)	79	May–Oct 2009	0.11	-	Obs	Muskala et al. (2015)
Gaik-Brzezowa (Poland)	80	May–Oct 2009	0.19	-	Obs	Muskala et al. (2015)
Developed in Finland	-	-	-	-	Glob Mod	Vuollekoski et al. (2015)
Developed in France	-	-	-	-	Glob Mod	Beysens (2016)
Paris (France)	63	April 2011–Mar 2012	0.055	-	Obs	Beysens et al. (2017)
Beiteddine (Lebanon)	123	2013–2014 growing seasons	0.13	0.46	Obs	Tomaszkiewicz et al. (2017)
Maktau (Kenya)	262	April 2016–Mar 2017	0.067/OPUR	> 0.2 mm	Obs/Mod	Tuure et al. (2019)

S.1. Detailed Model description

The original model setup was made suitable for a global contest; i.e. it included polar regions. Therefore, it included the water phase change between liquid and solid; i.e. vapour-to-liquid (condensation) and vapour-to-solid (desublimation). This was not changed in our modified version of the model for Iran because we presume desublimation might happen in some regions of Iran (e.g. in the mountain regions or north Iran). We also did not change the type and condition of the condenser material; it was assumed a horizontally aligned sheet of a suitable material such as low-density polyethylene (LDPE) or polymethylmethacrylate (PMMA). The condenser sheet was also assumed to be at 2 meters from the ground and thermally insulated from the ground.

$$\frac{dT_c}{dt}(C_c m_c + C_w m_w + C_i m_i) = P_{rad} + P_{cond} + P_{conv} + P_{lat} \quad (1)$$

The model was setup so that it assumes similar conditions for the phase-change of pre-existing water or ice on the condenser sheet. For instance, if the water on the condenser is in liquid phase (i.e. $m_w > 0$) and the condenser temperature $T_c < 0$ *℃,* then the sheet is losing energy (i.e. the right-hand side of Eq. (1) is negative). In that case, instead of solving Eq. (1), T_c is assumed to be constant and the lost mass from the liquid phase of water is transferred to the cumulated mass of ice; i.e. the water is transformed from liquid phase to solid phase. Consequently, Eq. (1) is replaced by

$$L_{wi}\ \frac{dm_w}{dt} = P_{rad} + P_{conv} + P_{lat}, \quad (2)$$

where L_{wi} is the latent heat of fusion. If the water on the condenser is in solid phase (i.e. $m_i > 0$) and the condenser temperature $T_c > 0$ *℃*, a similar equation is assumed for the change rate of ice mass (m_i).

Note that Eq. (2) is not related to the condensation of water; it only describes the phase change of the already condensed water or ice on the condenser. For the water condensation rate, which is assumed independent of Eq. (2), the mass-balance equation is then assumed as

$$\frac{dm}{dt} = \max\left[\ 0\ ,\ S_c k\left(P_{sat}(T_d) - P_c(T_c)\right)\ \right], \quad (3)$$

where m represents either the mass of ice (m_i) or water (m_w) depending on weather T_c is below or above 0 *℃*. $P_{sat}(T_d)$ is the saturation pressure at the dew point temperature and $P_c(T_c)$ is the vapor pressure over the condenser sheet. $k = h / L_{vw}\gamma = 0.622h / C_a p$ is the mass transfer coefficient, where L_{vw} is the specific latent heat of water vaporization, γ is the psychrometric constant, C_a is the specific heat capacity of air, and p is the atmospheric air pressure. Here, $h = 5.9 + 4.1\ u\ (511 + 294) / (511 + T_a)$ is the heat transfer coefficient, where u and T_a are the prevailing horizontal wind speed and the ambient temperature at 2 meters from the ground.

In practice, the wettability of the surface affects the vapor pressure P_c directly above it. In other words, P_c is lower over a wet surface; and thus, condensation may take place even if $T_c > T_d$. It is also assumed that the processes included in Eq. (3) undergo irreversible condensation; i.e. there is no evaporation or sublimation during daytime even if $T_c > T_a$. Furthermore, the model simulation resets the cumulative values for water and ice condensation at noon and takes the preceding maximum value of $m_w + m_i$ as the representative daily yield. This way, the model simulation replicates the daily manual dew water collection of the condensed water around sunrise; i.e. after which T_c is often above the dew point temperature. All terms and nomenclature are described in more details in Table S1 and Table S2.

The model output is dew formation yield given in liters of water collected on a 1 m^2 condenser sheet (i.e. L/m^2). However, this can be converted to units of mm (i.e. equivalent to rainfall). The model input parameters include: horizontal and vertical wind components at 2 meters, surface roughness (z_0), ambient temperature and dew point (T_a and D_P) at 2 meters,

short-wave and long-wave surface solar radiation (R_{sw} and R_{lw})

As we mentioned in the method section of manuscript and according to the ECMWF ERA-INTRIM data-base, the horizontal wind components (U_{10} and V_{10}) are provided at 10 meters. Therefore, the wind speed at 2 meters was calculated by using a logarithmic wind profile

$$WS = \frac{log\left(\frac{2+z_0}{z_0}\right)}{log\left(\frac{10+z_0}{z_0}\right)} \sqrt{U_{10}^2 + V_{10}^2}, \quad (4)$$

where z_0 is the surface roughness and U_{10} and V_{10} are the horizontal wind speed components at 10 meters. It is important to understand that Eq. (4) is valid during certain conditions. For instance, in stable conditions (such as at night) Eq. (4) it overestimates the wind speed at 2 meters whereas in unstable conditions it underestimates the wind speed at 2 meters.

According to the ECMWF ERA-INTRIM data-base, z_0 is obtained as an instantaneous forecast parameter whereas R_{sw} and R_{lw} are accumulated forecasted fields. The mean R_{sw} and R_{lw} in a time interval is obtained by taking the difference of the accumulated values between the corresponding time steps divided by the time difference in seconds. The result is a mean value for that time interval 00:00 or 12:00. All input parameters had a horizontal resolution 0.25 degree (approximately 30 km).

Table S2: Description of the dew formation model by listing the terms in Eq. (1).

Term	**Unit**	**Description**
dT_c/dt	K s^{-1}	Change rate of the condenser temperature
T_c	K	Temperature of the condenser
t	s	Time. Here the time step in the model was 10 s
C_c	J kg^{-1} K^{-1}	Specific heat capacity of the condenser. For low-density polyethylene (LDPE) and polymethylmethacrylate (PMMA) it is 2300 J kg^{-1} k^{-1}
C_i	J kg^{-1} K^{-1}	Specific heat capacity of ice (2110 J kg^{-1} k^{-1})
C_w	J kg^{-1} K^{-1}	Specific heat capacity of water (4181.3 J kg^{-1} k^{-1})
m_c	kg	Mass of the condenser given by $m_c = \rho_c S_c \delta_c$ where ρ_c, S_c, and δ_c are the density (here it is 920 kg m^{-3}), surface area (here it is 1 m^2), and thickness of the condenser (here it is 0.39 mm)
m_i	kg	Mass of ice
m_v	kg	Mass of water, representing the cumulative mass of water that has
P_{rad}	W	Heat exchange due to incoming and outgoing radiation $P_{rad} = (1 - a)\, S_c R_{sw} + \varepsilon_c S_c R_{lw} - S_c \varepsilon_c \sigma T_c^4$ where a is the condenser short-wave albedo (here it is 0.84), S_c is the condenser surface area (here it is 1 m^2), ε_c is the emissivity of the condenser (here it is 0.94), σ is Stephan-Boltzmann constant (5.67×10^{-8} W m^{-2} K^{-4}), T_c [K] is the temperature of the condenser, and R_{sw} and R_{lw} [W m^{-2}] are the incoming short-wave radiation (i.e. surface solar radiation downwards) and incoming long-wave radiation (i.e. surface thermal radiation downwards)
P_{cond}	W	Conductive heat exchange between the condenser surface and the ground. For simplicity, we assumed that the condenser is perfectly insulated from the ground; i.e. $P_{cond} = 0$
P_{conv}	W	Convective heat exchange $P_{conv} = S_c\,(T_a - T_c)\,h$ where S_c is the condenser surface area (here it is 1 m^2), T_a [K] is the ambient temperature at 2 meters from the ground, T_c [K] is the temperature of the condenser, and h [W m^{-2} K^{-1}] is the heat transfer coefficient that is estimated based on a semi-empirical equation (Richards, 2009) $h = 5.9 + 4.1\, WS\, (511 + 294) / (511 + T_a)$ and here WS [m s^{-1}] is the prevailing horizontal wind speed at 2 meters from the ground.
P_{lat}	W	Latent heat released by the condensation or desublimation of water $P_{lat} = \begin{cases} L_{vw} \dfrac{dm_w}{dt} & T_c > 0\ ^oC \\ L_{vi} \dfrac{dm_i}{dt} & T_c < 0\ ^oC \end{cases}$ where L_{vw} [J kg^{-1}] is the specific latent heat of water vaporization and and L_{vi} [J kg^{-1}] is specific latent heat of water desublimation. Here, dm_w/dt is the change rate of water whereas dm_i/dt is the change rate of ice

Table S3: A list of nomenclature.

Parameter	**Unit**	**Description**
α	--	Albedo of condenser sheet
C_a	J kg^{-1} K^{-1}	Specific heat capacity of air
C_c	J kg^{-1} K^{-1}	Specific heat capacity of the condenser
C_i	J kg^{-1} K^{-1}	Specific heat capacity of ice
C_{w}	J kg^{-1} K^{-1}	Specific heat capacity of water
DP	K	Dew point temperature
h	W K^{-1} m^{-2}	Heat transfer coefficient
k	Per s^{-1}	Mass transfer coefficient
L_{vi}	J kg^{-1}	Specific latent heat of desublimation for water
L_{vw}	J kg^{-1}	Specific latent heat of vaporization for water
L_{wi}	J kg^{-1}	Latent heat of fusion
m_c	kg	Mass of the condenser
m_i	kg	Mass of ice
m_w	kg	Mass of water
p	Pa	Atmospheric air pressure
p_c	Pa	Vapour pressure over condenser
p_{sat}	Pa	Saturation pressure of water
P_{cond}	W	Conductive heat exchange between the condenser surface and the ground
P_{conv}	W	Convective heat exchange
P_{lat}	W	Latent heat released by the condensation or desublimation of water
P_{rad}	W	Heat exchange due to incoming and outgoing radiation
R_{lw}	W m^2	Surface thermal radiation downwards
R_{sw}	W m^2	Surface solar radiation downwards
S_c	m^2	Surface area of condenser
T_a	K	Ambient temperature at 2 meters
T_c	K	Temperature of the condenser
U_{10}	m s^{-1}	Horizontal wind speed component at 10 meters
V_{10}	m s^{-1}	Horizontal wind speed component at 10 meters
WS	m s^{-1}	Prevailing horizontal wind speed at 2 meters
z_0	m	Surface roughness
δ_c	mm	Condenser sheet thickness
ε_c	--	Emissivity of condenser sheet
γ	Pa K^{-1}	Psychrometric constant
σ	W m^{-2} k^{-4}	Stefan-Boltzmann constant

S.2. Seasonal variation of cumulative dew yield

Figure S1, shows the seasonal occurrence of dew with a threshold less than 0.1 mm/day as the smallest amount of water can be collected on condenser sheet.

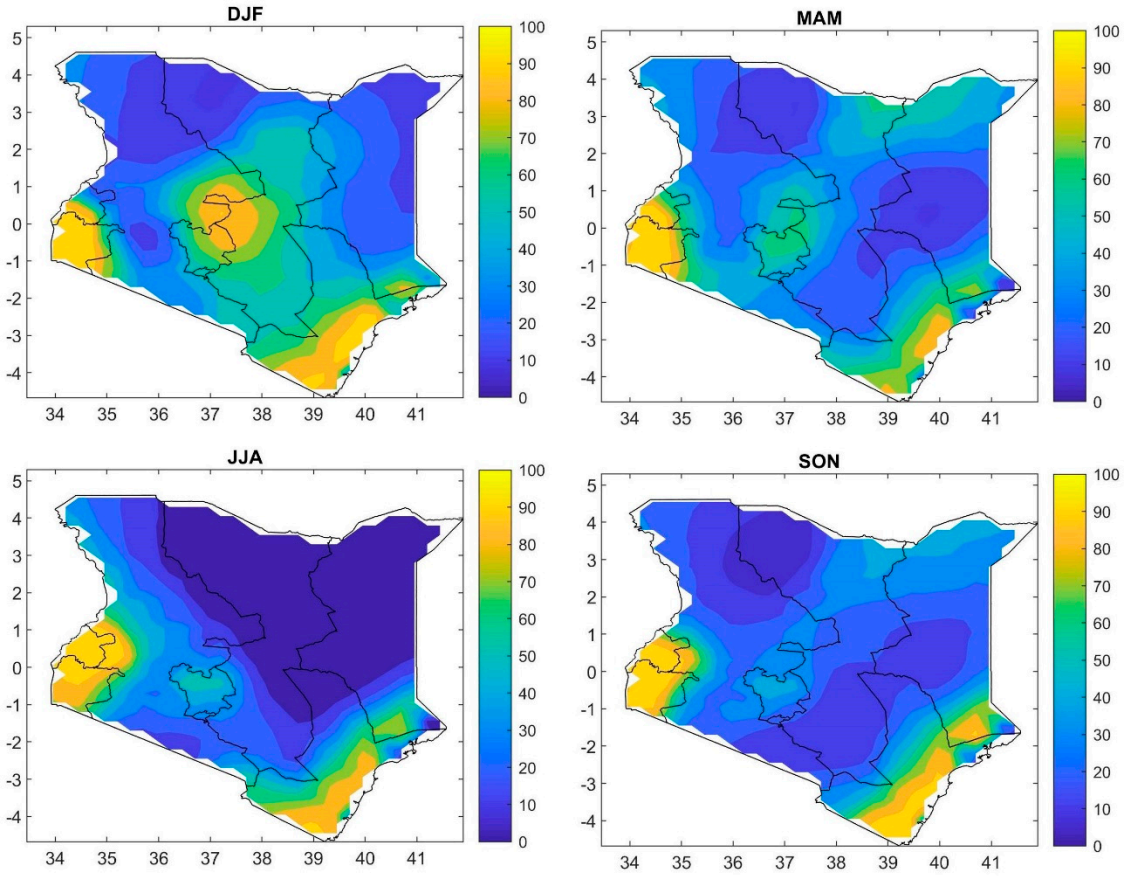

Figure S1: Spatial patterns for overall seasonal occurrence of dew formation days (with a threshold of 0.1 mm/day) represented by the percentage of the days per season during 1979–2018.

S.3. seasonal variation of meteorological parameters

Figure S2_S4 present the long-term mean seasonal variation of some key factors in dew formation (i.e., air temperature, dewpoint temperature, relative humidity, wind speed at 2-meter height and total cloud cover) in dew zone A, B and C respectively.

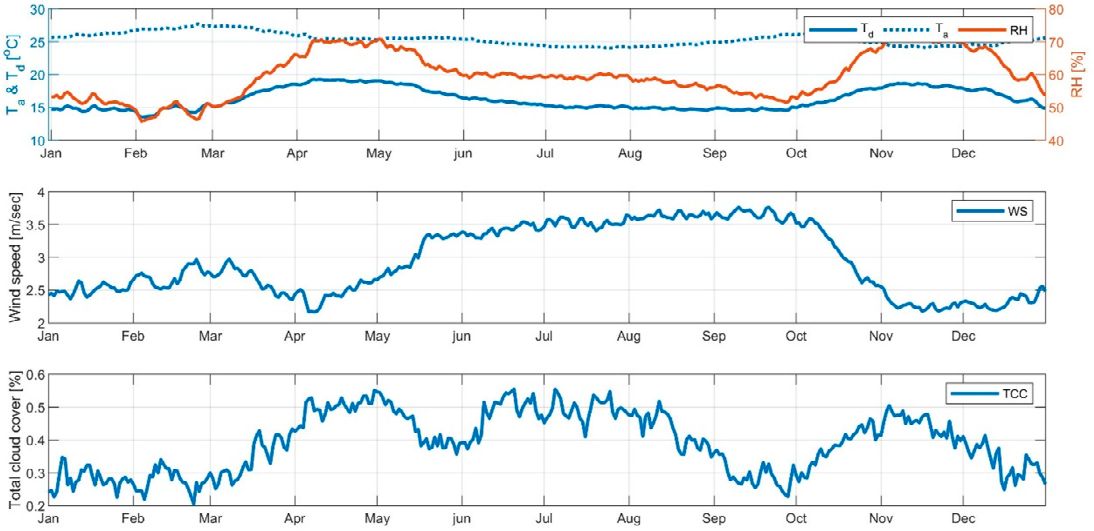

Figure S2. long-term mean seasonal variation in dew zone A. **a)** air temperature (point blue line), dewpoint temperature (solid blue line), relative humidity (red line), **b)** wind speed at 2 meter height (blue line) and **c)** total cloud cover (blue line).

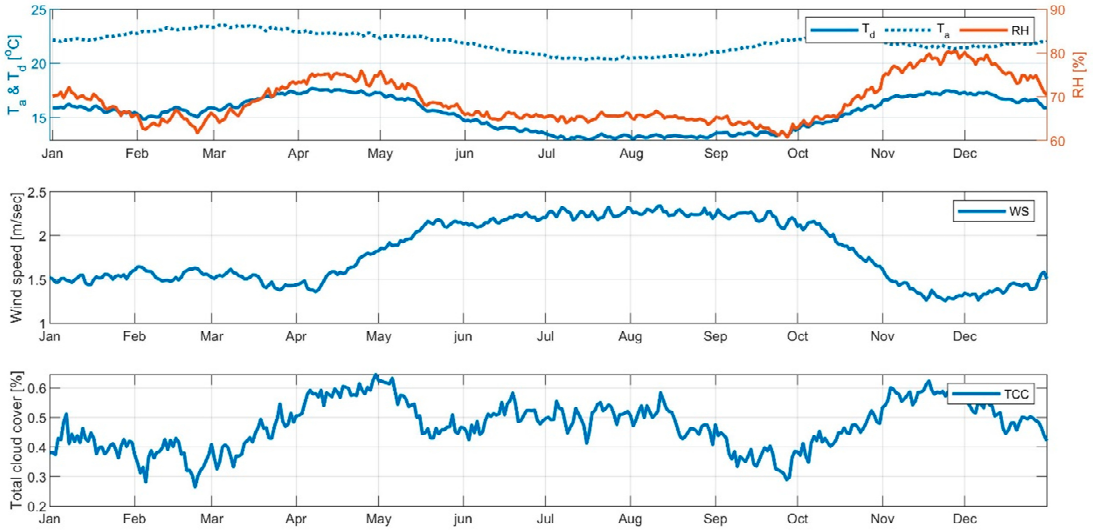

Figure S3. long-term mean seasonal variation in dew zone B **a)** air temperature (point blue line), dewpoint temperature (solid blue line), relative humidity (red line), **b)** wind speed at 2 meter height (blue line) and **c)** total cloud cover (blue line).

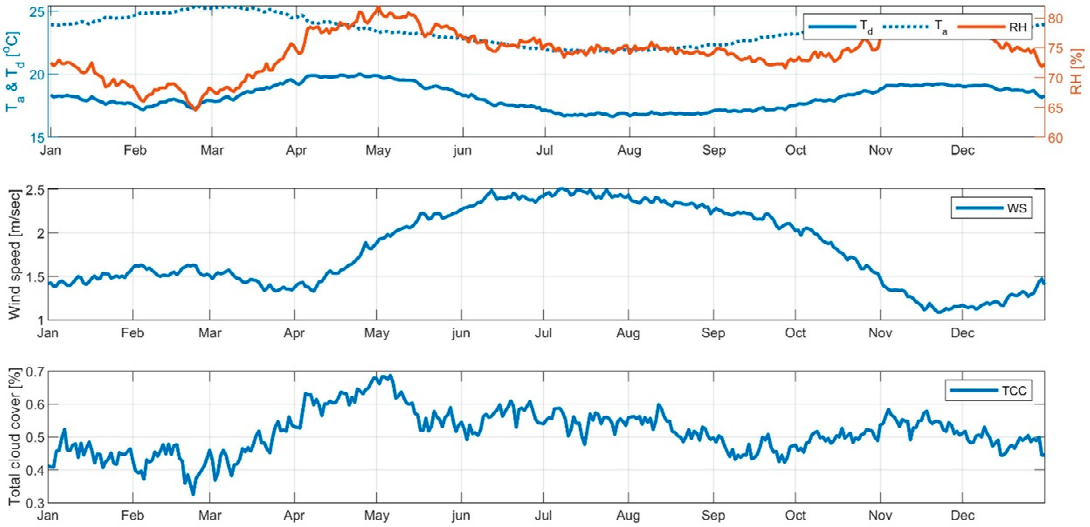

Figure S4. long-term mean seasonal variation in dew zone C **a)** air temperature (point blue line), dewpoint temperature (solid blue line), relative humidity (red line), **b)** wind speed at 2-meter height (blue line) and **c)** total cloud cover (blue line).

S.4. Dependency of dew yield on meteorological parameters

The correlation between dew yield and some of key meteorological factors in dew formation is presented in Figure S5_S7 for each dew zone, respectively.

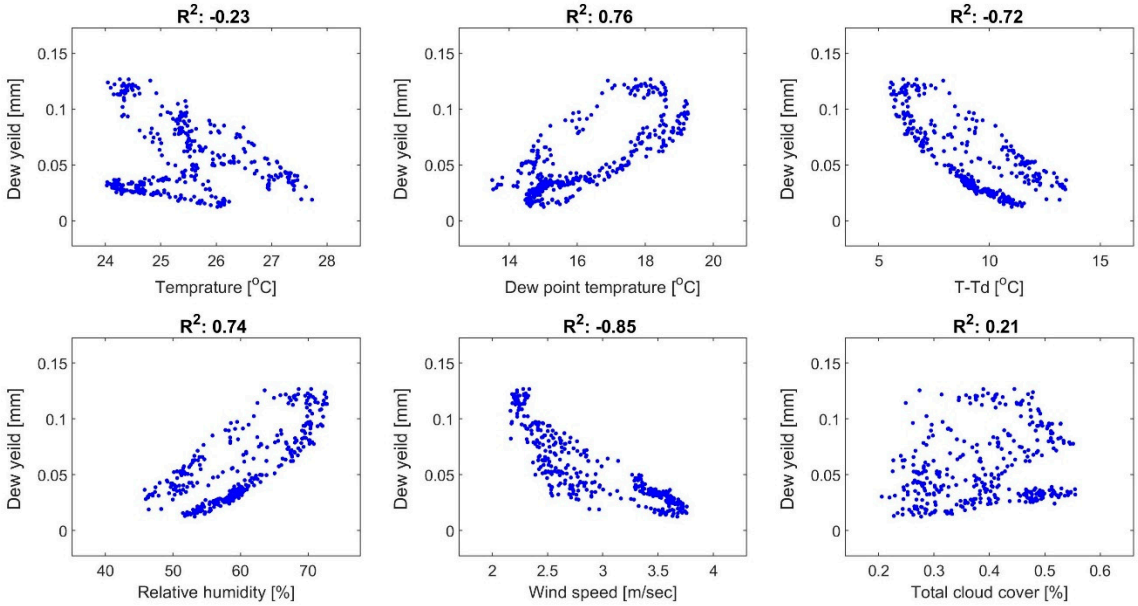

Figure S5. Correlation between dew yield (Y axis) and meteorological parameters (X axis) in dew zone A. **a)** Temperature, **b)** dewpoint temperature**, c)** difference between air temperature and dewpoint**, d)** relative humidity**, e)** wind speed at 2-meter height, and **f)** total cloud cover.

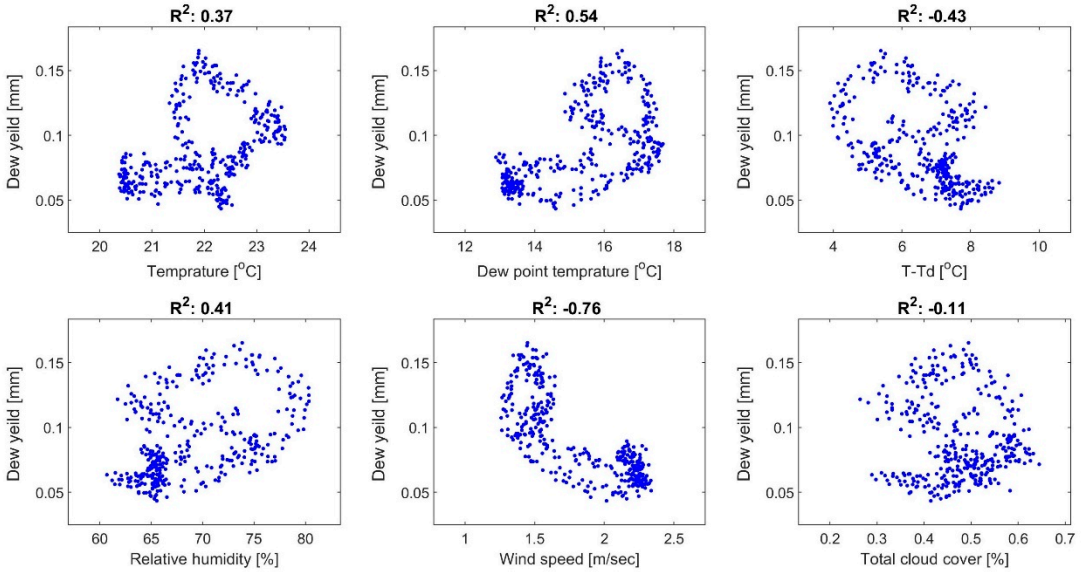

Figure S6. Correlation between dew yield (Y axis) and meteorological parameters (X axis) in dew zone B. **a)** Temperature, **b)** dewpoint temperature**, c)** difference between air temperature and dewpoint**, d)** relative humidity**, e)** wind speed at 2-meter height, and **f)** total cloud cover.

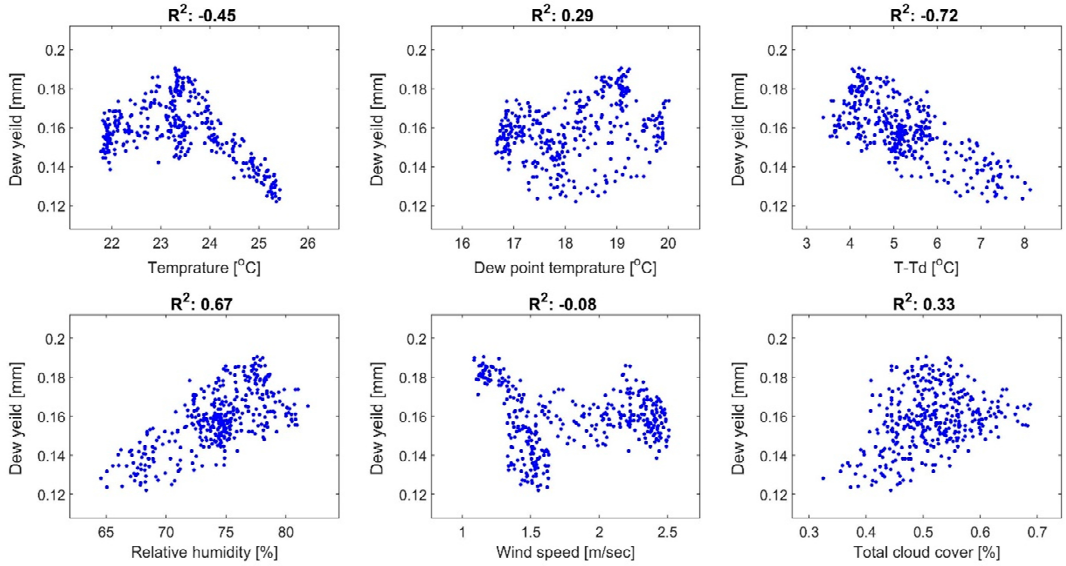

Figure S7. Correlation between dew yield (Y axis) and meteorological parameters (X axis) in dew zone C. **a)** Temperature, **b)** dewpoint temperature**, c)** difference between air temperature and dewpoint**, d)** relative humidity**, e)** wind speed at 2-meter height, and **f)** total cloud cover.

References

Arias-Torres, J.E., Flores-Prieto, J.J., 2016. Winter dew harvest in Mexico City. Atmosphere. 7(1), 2.

Berkowicz, S., Beysens, D. N., Milimouk, I., Heusinkveld, B., Muselli, M., Jacobs, A., Clus, O., 2007. Urban dew collection in Jerusalem: A three-year analysis. Proceedings of the 4th Conference on Fog, Fog Collection and Dew, Cape Town, South Africa.

Beysens, D., 2016. Estimating dew yield worldwide from a few meteo data. Atmospheric research. 167, 146-155.

Beysens, D., Milimouk, I., Nikolayev, V., Muselli, M., Marcillat, J., 2003. Using radiative cooling to condense atmospheric vapor: A study to improve water yield. Journal of Hydrology. 276 (1), 1-632 11.

Beysens, D., Mongruel, A., Acker, K., 2017. Urban dew and rain in Paris, France: Occurrence and physico-chemical characteristics. Atmospheric Research. 189, 152-161.

Beysens, D., Muselli, M., Milimouk, I., Ohayon, C., Berkowicz, S. M., Soyeux, E., Mileta, M Ortega, P., 2006. Application of passive radiative cooling for dew condensation. Energy. 31(13), 2303-2315.

Beysens, D., Muselli, M., Nikolayev, V., Narhe, R., Milimouk, I., 2005. Measurement and modelling of dew in island, coastal and alpine areas. Atmospheric Research. 73(1), 1-22.

Beysens, D., Ohayon, C., Muselli, M., Clus, O., 2006. Chemical and biological characteristics of dew and rain water in an urban coastal area (Bordeaux, France). Atmospheric Environment. 40(20), 3710-3723.

Burlando, M., 2009. The synoptic-scale surface wind climate regimes of the Mediterranean Sea according to the cluster analysis of ERA-40 wind fields. Theoretical and applied climatology. 96(1-2), 69-83.

Clus, O., Lekouch, I., Muselli, M., Milimouk-Melnytchouk, I., Beysens, D., 2013. Dew fog and rain water collectors in a village of S-Morocco (Idouasskssou). Desalination and Water Treatment. 51, 4235 – 4238.

Clus, O., Ortega, P., Muselli, M., Milimouk, I., Beysens, D., 2008. Study of dew water collection in humid tropical islands. Journal of Hydrology. 361, 159 – 171.

Gałek, G., Sobik, M., Błaś, M., Polkowska, Ż., Cichała-Kamrowska, K., 2012. Dew formation and chemistry near a motorway in Poland. Pure and Applied Geophysics. 169(5-6), 1053-1066.

Gandhisan, P., Abualhamayel, H.I., 2005. Modelling and testing of a dew collection system. Desalination. 18, 47 – 51.

Guan, H., Sebben, M., Bennett, J., 2014. Radiative-and artificial-cooling enhanced dew collection in a coastal area of South Australia. Urban Water Journal. 11(3), 175-184.

Jacobs, A. F. G., Heusinkveld, B. G., Berkowicz, S. M., 2008. Passive dew collection in a grassland area, The Netherlands. Atmospheric Research. 87, 377–385.

Khare, P., Singh, S. P., Maharaj Kumari, K., Kumar, A., Srivastava, S. S., 2000. Characterization of organic acids in dew collected on surrogate surfaces. Journal of Atmospheric Chemistry. 37(3), 231-244.

Kidron, G. J., 1999. Altitude dependent dew and fog in the Negev Desert, Israel. Agricultural and Forest Meteorology. 96, 1-8.

Kidron, G. J., Starinsky, A., 2012. Chemical composition of dew and rain in an extreme desert (Negev): Cobbles serve as sink for nutrients. Journal of Hydrology. 420, 284-291.

Lekouch, I., Kabbachi, B., Milimouk-Melnytchouk, I., Muselli, M., Beysens, D., 2010. Influence of temporal variations and climatic conditions on the physical and chemical characteristics of dew and rain in South-West Morocco. 5th International Conference on Fog, Fog Collection and Dew, Münster, Germany, 25-30.

Lekouch, I., Lekouch, K., Muselli, M., Mongruel, A., Kabbachi, B., Beysens, D., 2012. Rooftop dew, fog and rain collection in southwest Morocco and predictive dew modeling using neural networks. Journal of Hydrology. 448, 60-72.

Maestre-Valero, J. F., Martínez-Alvarez, V., Baille, A., Martín-Górriz, B., Gallego-Elvira, B., 2011. Comparative analysis of two polyethylene foil materials for dew harvesting in a semi-arid climate. Journal of Hydrology. 410, 84–91.

Mileta, M., Muselli, M., Beysens, D., Berkowicz, S. M., Heusinkveld, B. G., Jacobs, A. F. G., 2004. Comparison of dew yields in four Mediterranean sites: similarities and differences. 3th International Conference on Fog, Fog Collection and Dew (p. E2). University of Pretoria, South Africa.

Muselli, M., Beysens, D., Marcillat, J., Milimouk, I., Nilsson, T., Louche, A., 2002. Dew water collector for potable water in Ajaccio (Corsica Island, France). Atmospheric Research. 64, 297–312.

Muselli, M., Beysens, D., Mileta, M., Milimouk, I., 2009. Dew and rain water collection in the Dalmatian Coast, Croatia. Atmospheric Research. 92, 455-463.

Muselli, M., Beysens, D., Soyeux, E., Clus, O., 2006. Is dew water potable? Chemical and biological analyses of dew water in Ajaccio (Corsica Island, France). Journal of Environmental Quality. 35(5), 1812-1817.

Muskala, P., Sobik, M., Błaś, M., Polkowska, Ż., Bokwa, A., 2015. Pollutant deposition via dew in urban and rural environment, Cracow, Poland. Atmospheric Research. 151, 110-119.

Nilsson, T. M. J, Vargas, V. E., Niklasson, G. A., Granqvist, C. G., 1994. Condensation of water by radiative cooling. Renewable Energy. Vol.5, Part I, 310-317, Elsevier Science.

Nilsson, T., 1996. Initial experiments on dew collection in Sweden and Tanzania. Solar Energy Materials and Solar Cells. 40, 23-32.

Sharan, G., Beysens, D., Milimouk-Melnytchouk, I., 2007. A study of dew water yields on Galvanized iron roofs in Kothara (North-West India). Journal of Arid Environments. 69, 259 – 269.

Sharan, G., Clus, O., Singh, S., Muselli, M., Beysens, D., 2011. A very large dew and rain ridge collector in the Kutch Area (Gujarat, India). Journal of Hydrology. 405(1), 171-181.

Sobik, M., Blas, M., Polkowska, Z., 2010, July. Climatology of dew in Poland. 5th International Conference on Fog, Fog Collection and Dew. Münster, Germany.

Takenaka, N., Soda, H., Sato, K., Terada, H., Suzue, T., Bandow, H., Maeda, Y., 2003. Difference in amounts and composition of dew from different types of dew collectors. Water, Air, and Soil Pollution. 147(1-4), 51-60.

Tomaszkiewicz, M., Abou Najm, M., Zurayk, R., El-Fadel, M., 2017. Dew as an adaptation measure to meet water demand in agriculture and reforestation. Agricultural and Forest Meteorology. 232, 411-421.

Unal, Y., Kindap, T., Karaca, M., 2003. Redefining the climate zones of Turkey using cluster analysis. International Journal of Climatology: A Journal of the Royal Meteorological Society. 23(9), 1045-1055.

Vargas, W.E., Lushiku, E.M., Niklasson, G.A., Nilsson, T.M.J., 1998. Light scattering coatings: Theory and applications. Solar Energy Materials and Solar Cells. 54, 343-350.

Vuollekoski, H., Vogt, M., Sinclair, V. A., Duplissy, J., Järvinen, H., Kyrö, E. Makkonen, R., Petäjä, T., Prisle, N.L., Räisänen, P., Sipilä, M., Ylhäisi, J., Kulmala, M., 2014. Estimates of global dew collection potential. Hydrology and Earth System Sciense. 11, 9519-9549.

Wagner, G. H., Steele, K. F., & Peden, M. E., 1992. Dew and frost chemistry at a midcontinent site, United States. Journal of Geophysical Research: Atmospheres. 97, 20591-20597.